Microporous and Mesoporous Materials 312 (2021) 110740

Contents lists available at ScienceDirect

Microporous and Mesoporous Materials

journal homepage: http://www.elsevier.com/locate/micromeso

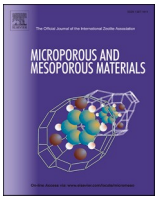

Novel periodic mesoporous organosilicas containing pyromellitimides and their application for the photodegradation of asphaltenes

Luana dos Santos Andrade [a], Larissa Otubo [b], Bruna Castanheira [a], Sergio Brochsztain [a,*]

[a] Centro de Engenharia, Modelagem e Ciências Sociais Aplicadas, Universidade Federal do ABC, Brazil
[b] Instituto de Pesquisas Energeticas e Nucleares, Brazil

A B S T R A C T

Periodic mesoporous organosilicas containing pyromellitic diimide units embedded in the pore walls (PMOPMI) were synthesized by co-condensation of the bridged silsesquioxane precursor N,N′-bis(3-triethoxysilylpropyl)pyromellitimide with tetraethoxysilane (TEOS) in acidic conditions, in the presence of the structure-directing agent Pluronics P-123. PMOPMI were also synthesized from the corresponding amic acid precursors. The PMOPMI were studied by different techniques, including N_2 adsorption isotherms, transmission electron microscopy, infrared and diffuse reflectance spectroscopy and contact angles. The studied samples displayed well-organized 2D-hexagonal structures. The PMOPMI were able to adsorb petroleum asphaltenes from toluene solutions, and were efficient photosensitizers for the photodegradation of the adsorbed asphaltenes when irradiated. Most of the asphaltenes were removed from solutions by the combined action of adsorption and photodegradation processes.

1. Introduction

Mesoporous organosilicas, hybrid organic-inorganic materials with organized pores and high specific surface areas, are very attractive supports for the introduction of organic functionalities [1–3]. Periodic mesoporous organosilicas (PMO) are a particular class of mesoporous organosilica where the organic modifier is inserted inside the pore walls, rather than in the pore interior, thus avoiding pore blocking [3–7]. Aromatic diimides, such as 3,4,9,10-perylenediimides (PDI) [8,9], 1,4,5,8-naphthalenediimides (NDI) [9,10] and pyromellitimides (PMI) [9], represent a very attractive class of compounds to incorporate into PMOs, since they can be easily functionalized with two opposite triethoxysilyl groups for condensation into the silica framework (Fig. 1A). Owing to their outstanding photochemical properties and strong electron acceptor character, aromatic diimides have been often employed in photocatalysis and organic electronics [11–13].

Our group has recently incorporated aromatic imides and diimides into mesoporous organosilicas by post-synthetic modification (grafting) [14–17]. This method, however, inserts the organic molecule in the pore interior (Fig. 1B), since the inorganic silica framework was pre-assembled, thus leading to partial pore blockage. In order to obtain PMOs with the organic groups inserted inside the pore walls, bridged silsesquioxanes are required, like the aromatic diimides of Fig. 1A. Furthermore, they should be added during the synthesis of the silica framework, usually together with a second silica source (co-condensation method). After extensive literature search, we found only four reports on PMO featuring aromatic imides as the organic group, two of them employing PDI [18,19] and the other two with NDI [20,21]. Therefore, to our knowledge, there are not previous reports on the synthesis of PMI-functionalized PMOs.

In the present work, we report for the first time the synthesis and characterization of PMO containing PMI units embedded in the pore walls (Scheme 1). The novel materials were named PMOPMI. The synthesis of PMOPMI was performed using N,N′-bis(3-triethoxysilylpropyl) pyromellitimide (PMI-BS) (**1A**) as a precursor, in the presence of tetraethoxysilane (TEOS) and surfactant Pluronics P-123, in conditions similar to the synthesis of SBA-15 [22]. PMI-BS, on its turn, was synthesized by reaction between pyromellitic dianhydride (PMDA) and 3-aminopropyltriethoxysilane (APTES). Hydrolysis of the silane groups was observed during the synthesis of PMI-BS, so that the actual precursor used in the synthesis of PMOPMI was the -$Si(OH)_3$ derivative (**1B**) (Scheme 1). The synthesis of PMOPMI was also carried out by a second method, using the corresponding amic acids as precursors, which are expectedly converted to PMI by ring closure during the hydrothermal PMO synthesis.

In order to demonstrate the potential of the PMOPMI for applications, we studied the adsorption and subsequent photocatalytic degradation of petroleum asphaltenes, in comparison to titanium dioxide, a benchtop photocatalyst. The adsorption and photochemical degradation of petroleum asphaltenes is of great interest for issues such as oil

* Corresponding author. Avenida dos Estados, 5001, 09210-170, Santo Andre, Brazil.
E-mail address: sergio.brochsztain@ufabc.edu.br (S. Brochsztain).

https://doi.org/10.1016/j.micromeso.2020.110740
Received 29 August 2020; Received in revised form 23 October 2020; Accepted 29 October 2020
Available online 3 November 2020
1387-1811/

upgrading and the remediation of oil spills. Our results showed a better performance for the PMOPMI than that of commercial TiO_2.

2. Experimental part

Materials. Pluronic P-123, tetraethoxysilane (TEOS), 3-aminopropyltriethoxysilane (APTES) and pyromellitic dianhydride (PMDA) were supplied by Sigma-Aldrich. Titanium dioxide (TiO_2) was from Degussa, consisting of a mixture of anatase and rutile phases (80:20). Deuterated dimethylsulfoxide (DMSO-d_6) was obtained from Merck. Hydrochloric acid, ethanol and toluene were purchased from JT Baker (all solvents were HPLC-grade). Petroleum ether (30–70 °C) and *n*-heptane (both analytical grade) were obtained from Labsynth. Aqueous solutions were prepared with deionized water. Non-modified SBA-15 was synthesized according to the previously reported method [22]. A sample of PMO containing 8 wt% NDI (PMONDI), synthesized according to our recent report [20], was already available in our laboratory. Petroleum asphaltenes were isolated from a sample of petroleum of Campos basin (Brazil), using the SARA procedure (IP-143), which consists in precipitation with *n*-heptane (800 mL heptane for 20 g of petroleum). The syntheses of PMOPMI precursors N,N′-bis(3-triethoxysilylpropyl)-pyromellitimide (PMI-BS) (**1A**), N,N′-bis(3-trihydroxysilylpropyl)-pyromellitimide (**1B**) and amic acids (**2**) are given as supplementary information (Scheme S1), and their structures were confirmed by ^{1}H NMR and UV–visible spectra [23] (Figures S1, S2 and S3).

Synthesis of PMOPMI-1 (starting from diimide precursor). Pluronics (4.1 g) was stirred for 1 h in 30 mL water, until complete dissolution. 100 mL of HCl 2 M were added, and the mixture was stirred for additional 20 min. The solution was placed in an oil bath (35 °C) and TEOS (9.2 mL, 42 mmol) was added, followed by hydrolyzed PMI-BS (**1B**) (0.25 mmol) (Table 1), which was dissolved in 0.5 mL DMSO-d_6, as described in Method I (Scheme S1). The mixture was stirred for 24 h at 35 °C, and then transferred to a mini-autoclave and heated for additional 24 h at 100 °C. After cooling down, water (2 L) was added and the resulting white solid was filtered off in Buchner. The solid was washed twice with a mixture of ethanol (500 mL) and HCl 2 M (20 mL), filtered off and dried under vacuum. The material was finally extracted for 48 h with ethanol in a soxhlet extractor, in order to remove the template (Pluronics). The sample was named PMOPMI-1, since it arose from Method I.

Synthesis of PMOPMI-2 (starting from amic acid precursors). The material was synthesized using the same procedure as for PMOPMI-1, except for the precursor added to the reaction. For PMOPMI-2, the DMSO precursor solution from Method II, containing 30% PMI-BS + 70% amic acids (Scheme S1), was added to the reaction mixture after TEOS. The amounts of reagents used for the synthesis of the PMOPMI are summarized in Table 1.

Instruments. ^{1}H NMR spectra were registered with a Varian VNMRS 500 MHz spectrometer. Absorption spectra were obtained with a Varian Cary 50 UV–visible spectrophotometer. Diffuse reflectance spectroscopy (DRS) was also performed with the Cary-50, using the optical fiber external probe (Barrelino accessory). Nitrogen adsorption isotherms were performed with a Nova 2200 Surface Area and Pore Size Analyzer (Quantachrome). Specific surface areas were obtained with the BET method, and pore size distributions (PSD) with the BJH method (desorption branch). Pore volumes were obtained at $P/P_0 = 0.97$.

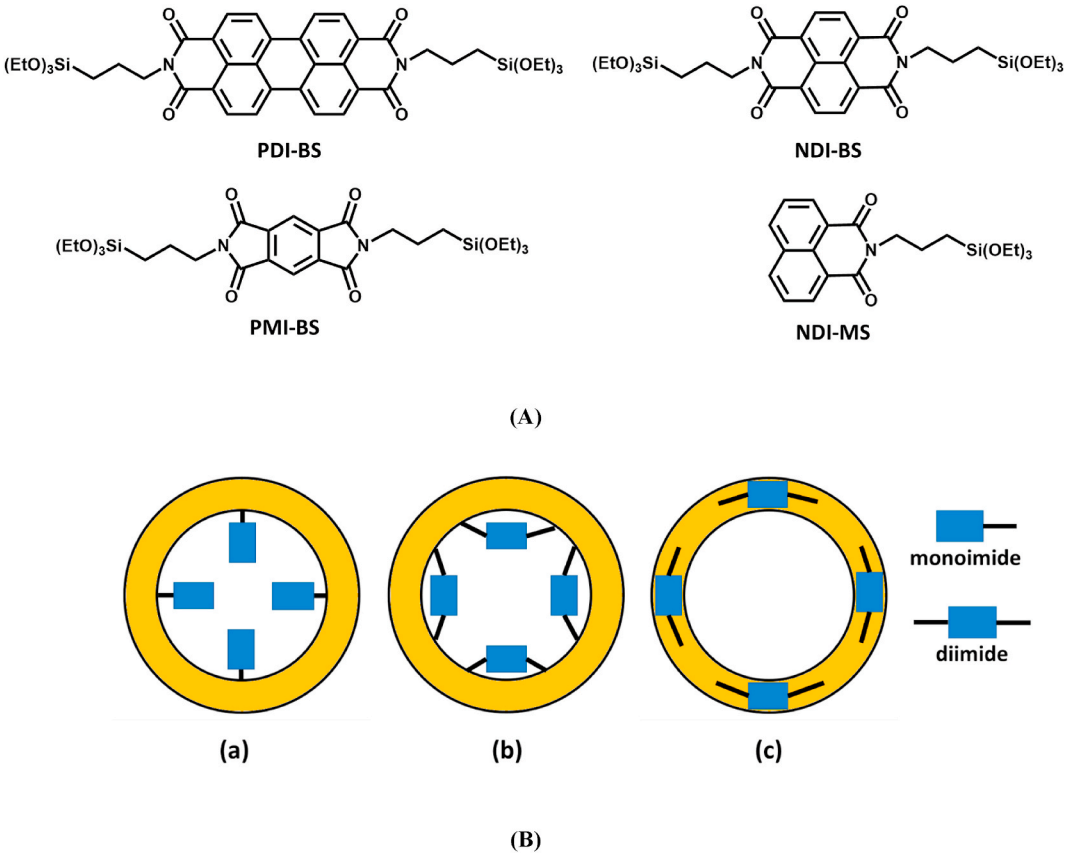

Fig. 1. (A) Structure of silsesquioxane aromatic imides which have been used as precursors for mesoporous organosilicas: N,N′-bis(3-triethoxysilylpropyl)-3,4,9,10-perylenediimide (PDI-BS) [18,19]; N,N′-bis(3-triethoxysilylpropyl)-1,4,5,8-naphthalenediimide (NDI-BS) [20,21]; N,N′-bis(3-triethoxysilylpropyl)-pyromellitimide (PMI-BS) (this work); N-(3-triethoxysilylpropyl)-1,8-naphthalimide (NDI-MS) [17] (a monoimide). (B) Placing of the aromatic imides in mesoporous organosilicas for different synthetic strategies: (a) Monoimides (regardless of method). (b) Diimides (grafting). (c) Diimides incorporated into PMO (co-condensation using bridged silsesquioxanes).

Micropore volumes and areas were calculated between $P/P_0 = 0.2–0.5$ using the t-plot method. Transmission electron microscopy (TEM) images were recorded with a JEOL microscope operating at 200 kV. Contact angles were measured on the pressed PMOPMI powders with an Attension Theta Optical Tensiometer (KSV). The tensiometer features a digital camera which records drop images and analyses their shapes with the included software (OneAttension v2.2). The images were recorded immediately after drop deployment from the needle tip, using the automatic trigger of the equipment. Infrared spectra were carried out at the Analytical Center of University of Sao Paulo (CA-USP), using KBr pellets, in a PerkinElmer Frontier FTIR. Elemental analysis (CHN) was also performed at CA-USP.

Photocatalytic experiments. Irradiation was performed using an Omnicure S1000 Hg lamp (100 W, bandpass filter: 320–500 nm), containing an optic fiber guide. For the irradiation experiments, 15 mg of catalyst were added to 5 mL of 400 mg/L asphaltene solutions in toluene. The samples were stirred in the dark for 24 h to ensure asphaltene adsorption equilibrium. After this period, the Hg lamp was turned on, with the tip of the optic fiber guide positioned 5 cm above the surface. The temperature was kept at 26 °C during irradiation, using a water bath. Asphaltene concentration was determined after certain time intervals (0, 15, 30, 60, 120, 180, 240 and 300 min). For this purpose, the samples were centrifuged (5000 rpm, 5 min), and aliquots of 100 μL were collected from the supernatant and diluted in 3 mL of toluene for UV/Vis analysis. The asphaltene concentration was obtained from the absorbance at 400 nm, in comparison to a standard curve (Fig. S4). Direct asphaltene photolysis was performed with an 80 mg/L asphaltene initial concentration.

3. Results and discussion

Synthesis of PMO precursors. After extensive literature survey, we found only two reports on the synthesis of PMI-BS (**1A**). Wengrovius et al. reported in 1994 a failed attempt to obtain the compound [24]. About 20 years later, Pfeifer et al. were able to obtain PMI-BS using Gabriel synthesis [25]. It is also worth mentioning the report by Hobson and Shea (1997) [26], who synthesized a series of bridged diimide silsesquioxanes by transimidation, although the series did not include pyromellitimides.

Table 1
Amounts of organic and inorganic precursors added to the synthesis of PMOPMI.

Sample	TEOS	PMI precursor[a]	PMI/TEOS	
			Mole ratio	Weight ratio[b]
PMOPMI-1	42 mmol	0.25 mmol	0.6%	4%
PMOPMI-2	42 mmol	1 mmol	2.4%	16%

[a] Organic precursor (see Scheme S1): hydrolyzed PMI-BS (**1B**) for PMOPMI-1; amic acids (**2**) for PMOPMI-2.
[b] Considering full hydrolysis and condensation of the precursors.

We employed here two different methods in attempt to obtain PMI-BS (Scheme S1): Method I, employing stoichiometric amounts of the reagents and DMSO as the solvent, and Method II, using excess APTES, where the APTES works both as a reagent and as a solvent. Method II has been employed recently by our group to synthesize the related naphthalenediimide derivative (NDI-BS) [20,21], and by other authors for the corresponding perylenediimide derivative (PDI-BS) (Fig. 1A) [27,28]. In both methods, the mixture was heated at 130 °C for a short time (less than 5 min). Heating for longer times resulted in condensation, leading to the formation of a gel, in agreement with Wengrovius' report [24].

The diimide was formed after 5 min of reaction with Method I, according to ^{1}H NMR (Figs. S1–A) and UV–visible spectra (Fig. S2), which agree with the reported spectra [23,25]. The ^{1}H NMR spectrum shows the expected aromatic singlet and the three methylene groups from the propyl chain. However, partial hydrolysis of the ethoxy groups occurred, as seen by the appearance of the signals of ethanol (3.43 and 1.04 ppm), replacing those of the ethoxy groups in **1A** (3.72 and 1.12 ppm). The extent of hydrolysis was estimated as 85% from the integrals. After aging for a week in the DMSO solution, hydrolysis was nearly complete, as seen in Figs. S1–B (the signals at 3.72 and 1.12 ppm were barely visible), giving compound **1B**, which was then employed for PMO synthesis. Since hydrolysis of the silane is the first step in PMO formation, it is not critical to employ **1B** as a precursor rather than **1A**.

When we used Method II, however, the reaction did not go to completion, as observed in the ^{1}H NMR spectrum in Fig. S3. We obtained *ca.* 30% PMI-BS, while the remaining 70% consisted of a mixture of amic

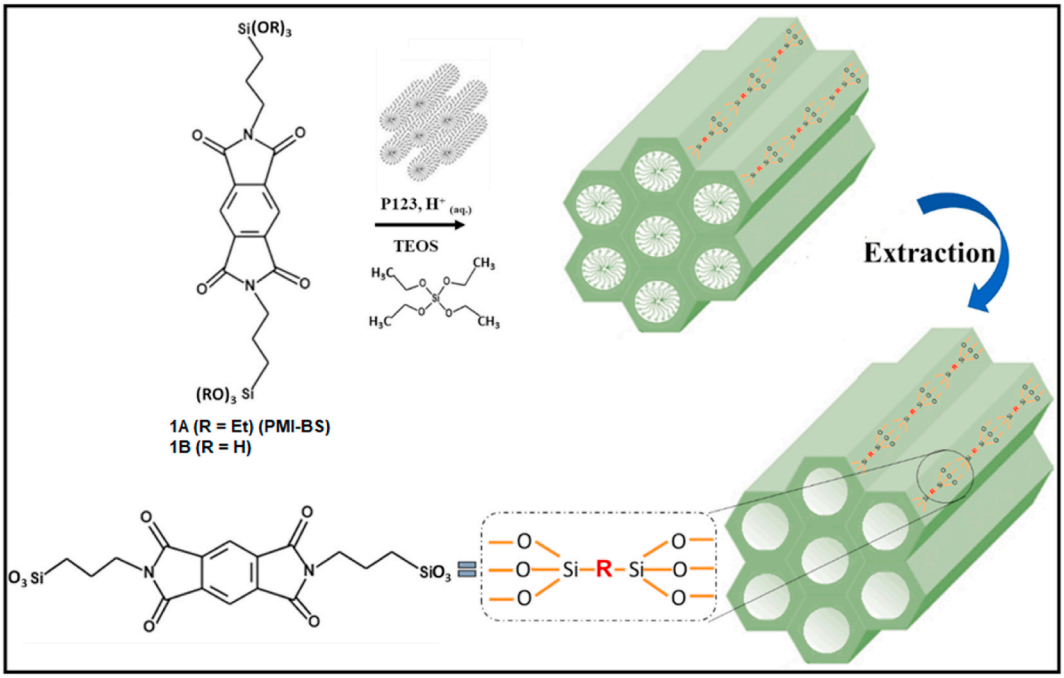

Scheme 1. Synthesis of PMOPMI via diimide precursors.

acids (**2**) (Scheme S1, right side), as confirmed by comparison with published spectra [29]. The amic acids are the ring opened intermediates in the imide formation reaction. The imide **1** and the amic acid **2** are easily distinguishable in the ^{1}H NMR spectrum by the N–CH_2-protons, which lie at 2.79 ppm in the former and at 3.17 in the latter, and by the aromatic proton region. Partial hydrolysis (≈10%) of the ethoxy groups occurred in this reaction as well, although to a lesser extent than Method I. These results suggest that DMSO is a better solvent than APTES for the reaction, perhaps due its higher polarity. The use of APTES, on the other hand, resulted in a lesser extent of silane hydrolysis.

We then decided to use this mixture containing **1** + amic acids **2** as precursors for PMOPMI. It is well known that amic acids are converted to imides by ring-closure (with loss of water) when heated. Polymer chemists usually polymerize the amic acids, which are easier to process, and then convert the polyamic acids to polyimides by annealing at high temperatures. Polypyromellitimide-silica hybrids have been prepared by this route [29–32]. In addition, acidic media favors ring closure. Thus, all the conditions used in the hydrothermal synthesis of the PMO are favorable to imide formation, and all the intermediates **2** in Scheme S1 would expectedly be converted to PMI units when incorporated to the PMO. Using amic acids as precursors might result in PMOs with different properties as compared to pure imide precursors. The more flexible amic acid chains will be present during the initial condensation steps, which take place at room temperature, but later on will shrink as they lose water and the rings close in the hydrothermal conditions, what could affect the porosity.

Synthesis and characterization of PMOPMI. The PMOPMI were synthesized by co-condensation with TEOS, in conditions analogue to those typically used in the synthesis of SBA-15 [20,22]. We obtained well-organized 2D-hexagonal silica, regardless of using **1** or **2** as a precursor, as seen in the TEM images in Fig. 2. The PMOPMI were composed by regular rods 200–300 nm wide and *ca.* 1 μm long, with well-aligned pores parallel to the long axis, and fused to each other by the ends (and laterally in some cases). Some free ends with hexagonal shape and hexagonal pore arrangement can be observed. Additional TEM images are shown in Fig. S5.

Nitrogen adsorption isotherms for the PMOPMI are shown in Fig. 3, and the corresponding textural parameters are given in Table 2. The isotherms are of type IV(a) with H1 hysteresis, typical of 2D-hexagonal organosilicas of the SBA-15 family [33]. Note that the pore sizes of PMOPMI were nearly the same as pristine SBA-15 (Table 2), indicating that the diimides were indeed inserted within the walls, resulting in no pore blocking (Fig. 1B). Furthermore, the sample PMOPMI-2, which was synthesized from the amic acid mixture, presented higher surface area and pore volume and a wider pore size distribution than PMOPMI-1 (Fig. 3B), synthesized from the diimide precursor. This finding could be due to extra void space within the walls generated as the amic acid molecules undergo ring closure to the less bulky imide molecule, releasing water. This is in agreement with the higher micropore area of PMOPMI-2 relative to PMOPMI-1, as calculated by the t-plot method.

Micropore analysis (Table 2) showed a great decrease in the micropore volume and area of the PMOPMI in comparison to pristine SBA-15.

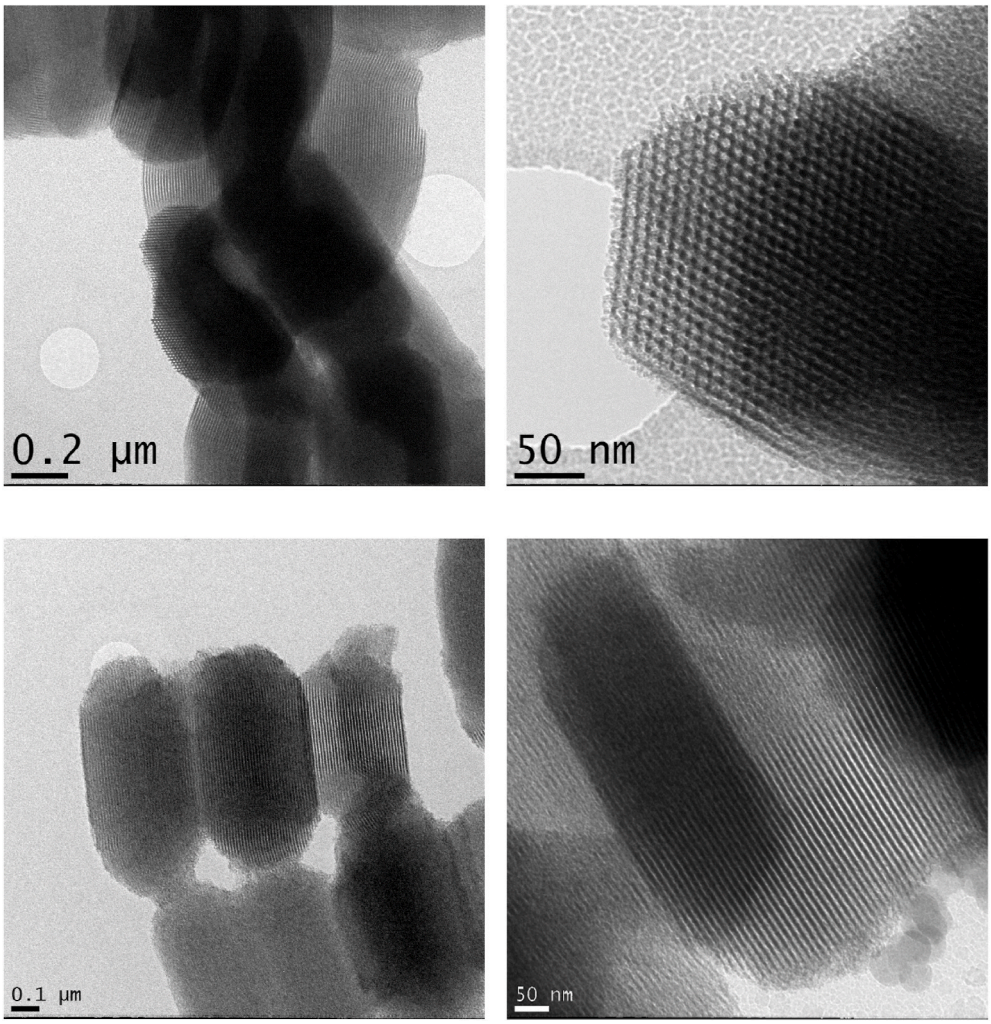

Fig. 2. TEM images of PMOPMI-1 (top) and PMOPMI-2 (bottom).

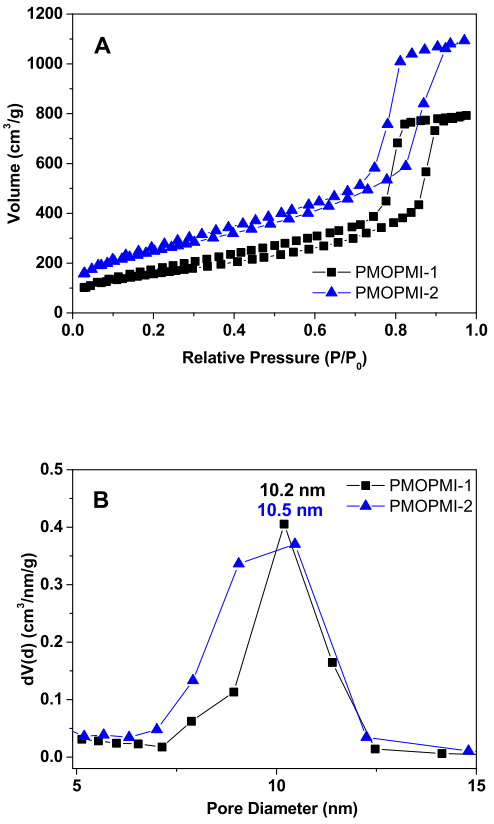

Fig. 3. (A) Nitrogen adsorption isotherms of the PMOPMI samples. (B) Pore size distribution of the PMOPMI samples from BJH method (desorption branch).

Table 2
Textural properties of SBA-15 and PMOPMI samples.

Sample	S_{BET}[a]	V_{pore}[b]	pore size[c]	micropores[d]	%C[e]	CA[f]
SBA-15	631	1.07	10.2	0.079 (174)	0.4%	11.4°
PMOPMI-1	566	0.97	10.2	0.003 (19)	4.5%	32.9°
PMOPMI-2	892	1.23	10.5	0.016 (50)	3.5%	33.4°

[a] Specific surface area (m^2/g).
[b] Total pore volume (cm^3/g), calculated at $P/P_0 = 0.97$.
[c] Pore diameter (nm) from BJH method (desorption branch).
[d] Micropore volume (cm^3/g) and area (m^2/g) (values in parenthesis) calculated with t-plot.
[e] Carbon content from elemental analysis.
[f] Contact angle (average of right and left contact angles).

The micropores in SBA-15 originate from the poly-ethylene oxide chains of the Pluronic micelles, and are found perforating the walls [22]. Therefore, the decrease in micropore volume and area is another evidence that the organic PMI groups are inside the walls in the PMOPMI.

We further characterized the PMOPMI by elemental analysis, contact angle and infrared spectroscopy. The elemental analysis (Table 2) showed between 3.5 and 4.5% carbon, which is consistent with the added amount of precursors, supporting the successful incorporation of the organic groups into the PMOPMI. The contact angle of water droplets, measured on pellets of the compressed powders, showed an increase from 11° in pristine SBA-15 to 33° in the PMOPMI (Fig. 4, Table 2), indicating that the surface of the PMOPMI samples was more hydrophobic than inorganic SBA-15, thus confirming the incorporation of the organic groups. The infrared spectrum of PMOPMI-1 is shown in Fig. S6. Although the strong Si–O stretching band and its overtones cover most of the features of the organic molecules, the imide carbonyl stretching of the pyromellitimide can be seen as a shoulder at 1725

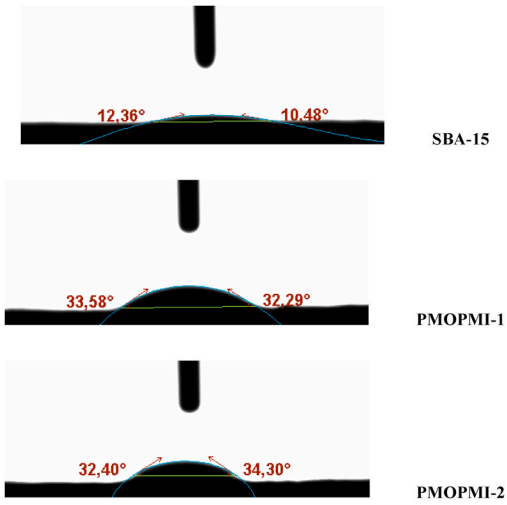

Fig. 4. Contact angle of water droplets on SBA-15, PMOPMI-1 and PMOPMI-2.

cm^{-1}. C–H stretch bands are also observed in the range 2800–3000 cm^{-1}.

Fig. 5 shows DRS spectra of the PMOPMI, as compared to the spectrum of the precursor PMI-BS in solution. As noticed, the absorption band centered at 307 nm in the precursor PMI-BS was split into two bands with maxima at 273 and 370 nm in the PMOPMI. We tentatively attribute this finding to exciton-splitting between neighboring PMI units within the PMO walls, showing that the diimide molecules are in close proximity in the materials.

Asphaltene removal by PMOPMI. Removal of asphaltenes from liquid streams is of great interest for several processes, ranging from the deasphalting of crude oil in refineries to the remediation of oil spills [34–36]. We have recently reported on the adsorptive capacity of PMONDI materials towards asphaltenes [34]. Thus, we studied the performance of the PMOPMI in asphaltene removal by the combined adsorption and photocatalytic processes (Fig. 6), in comparison to standard materials, namely, TiO_2 (Degussa) and pristine SBA-15. Before irradiation, the asphaltenes were adsorbed onto the different adsorbents by stirring the powders for 24 h in asphaltene solutions in toluene. Remarkably, the PMOPMI were able to remove virtually all the asphaltenes from solution by the combined effects of adsorption and photocatalysis, and in shorter times than the other adsorbents (Fig. 6).

Considering the adsorption process alone, the absorbance decay due

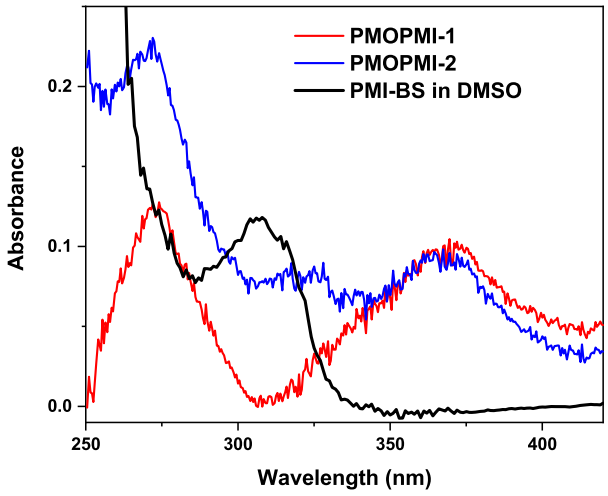

Fig. 5. DRS spectra of the PMOPMI samples in comparison to the solution spectrum of PMI-BS.

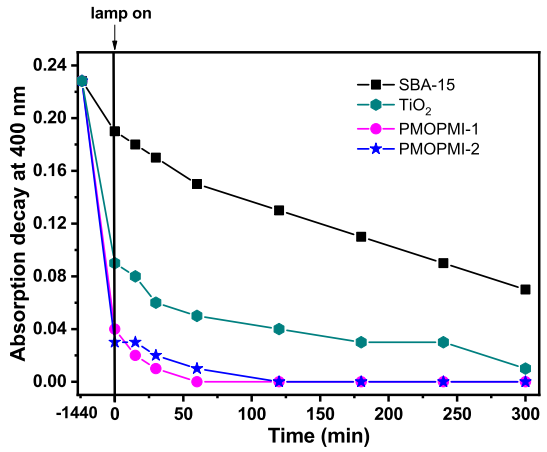

Fig. 6. Effect of the combined adsorption and photocatalytic processes in the removal of asphaltenes from toluene solutions by PMOPMI (monitored by the absorbance at λ = 400 nm), as compared to standard materials. The lamp was turned on at t = 0, so that negative time values correspond to asphaltene adsorption in the dark (see Fig. 7).

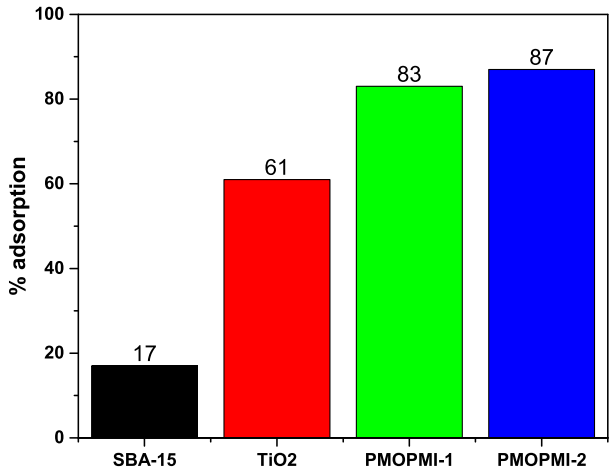

Fig. 7. Adsorption of asphaltenes from toluene solutions by the PMOPMI and by reference adsorbents, after 24 h stirring in the dark.

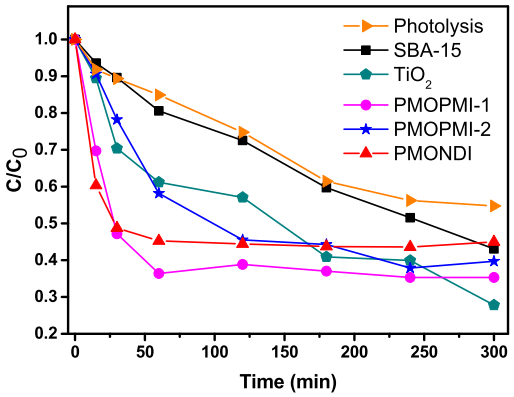

Fig. 8. Asphaltene degradation under irradiation as a function of time for the different systems.

to asphaltene adsorption in the dark can be seen in Fig. 6 (before turning on the lamp) and the adsorption data are summarized in Fig. 7. The higher adsorption capacity of TiO_2 in comparison to SBA-15, in spite of the former having a lower surface area, can be attributed to a higher surface acidity of TiO_2 [37]. It has been shown that a high surface acidity favors asphaltene adsorption [38]. The PMOPMI, on their turn, displayed a higher adsorptive capacity than inorganic TiO_2 and SBA-15, which can be attributed to the presence of the organic PMI moieties, rendering the adsorbent surface more hydrophobic, as indicated by the contact angle results. PMOs have been shown by other authors to be efficient adsorbents for organic pollutants [39,40]. Phenylene- and biphenylene-bridged PMOs [40–42], particularly, have been shown to be excellent adsorbents for polycyclic aromatic hydrocarbons such as naphthalene, anthracene and pyrene, which are often taken as asphaltene models.

The organized channels of mesoporous silica are very suitable hosts for photochemical reactions. Photocatalytic systems within mesoporous silica have been recently reviewed [43,44]. Fig. 8 shows the photocatalytic performance of the different materials after turning on the lamp (at t = 0, see Fig. 6), normalized to the initial absorbance ($A/A_0 = C/C_0$). A sample of PMONDI (PMO with 8% NDI by weight), from our previous work [20,34], was also tested. It can be noted that photodegradation in the presence of PMOPMI-1 and PMONDI was faster than with all the other catalysts.

Note that UV–visible absorbance is an indirect measure of the photodegradation rate, because the concentration of asphaltenes in the solution phase is monitored, whereas the photochemical reactions occur within the mesochannels. Most likely, the photodegradation products were desorbed from the silica surface, leaving room for new asphaltene molecules to adsorb, thus leading to the observed decrease of concentration in the solution phase (Fig. 8). However, elucidating the detailed photodegradation dynamics, which ought to be quite complex, is out of the scope of the present work.

Because the asphaltenes can absorb the light from the Hg lamp, as seen in Fig. S2, we also performed direct photolysis of the asphaltenes in homogeneous solution as a control. As seen in Fig. 8, photolysis catalyzed by PMOPMI and PMONDI was by far more efficient than direct photolysis (direct photolysis resulted in a degradation rate similar to SBA-15), stressing the important role of the diimide functionalities in the process.

Mechanism of asphaltene photodegradation. The photochemistry of aromatic diimides has been well documented [45–50]. They are known as efficient triplet photosensitizers, especially the NDI and PMI. In general, the perylenediimides are highly fluorescent in the monomeric form in solution. In contrast, the corresponding naphthalenediimides and pyromellitimides are only weakly fluorescent. The difference resides in the strong trend to intersystem crossing observed with the NDI and PMI, so generating triplet states in high yields under irradiation. ^{3}NDI and ^{3}PMI readily react with dissolved oxygen, generating oxygen reactive species (ORS) such as singlet oxygen and hydroxyl radicals, which will degrade the asphaltene molecules, in the so-called Type I mechanism (Scheme 2). Other authors have proposed such mechanism to explain dye degradation by NDI and PMI. The biological photoactivity of the aromatic diimides (antimicrobial, antiviral and antitumor) has also been attributed to damage to the DNA by ORS generation [45].

A second possible mechanism is via radical formation by electron transfer (Type II mechanism, Scheme 2). Aromatic diimides are excellent electron acceptors, forming stable anion radicals in the presence of electron donors [8–10,51]. In our system, polycyclic aromatic hydrocarbons (PAH) present in the asphaltenes could act as electron donors. The PMI radicals formed within the PMO walls could then act as initiators in radical chain degradation of asphaltenes. Radicals formed by oxidation of the PAH could also participate in the photodegradation process.

4. Conclusions

Pyromellitimide units were successfully inserted within the pore walls of periodic mesoporous organosilicas, resulting in the PMOPMI materials. The PMOPMI presented well organized 2D-hexagonal

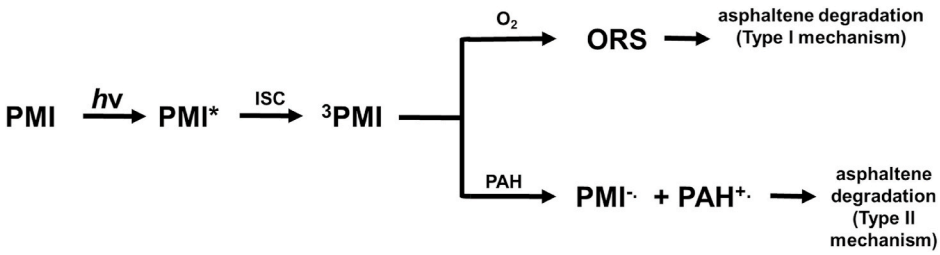

Scheme 2. Proposed mechanisms for asphaltene photodegradation in the presence of PMOPMI (the same mechanism also accounts for PMONDI activity). ISC: Intersystem crossing; ORS: oxygen reactive species; PAH: polycyclic aromatic hydrocarbons.

structures, showing that the presence of PMI did not disturb the mesostructure of the materials. Pore diameters of the PMOPMI were the same as the unmodified mesoporous silica, confirming that the PMI were indeed inside the walls, leaving the pores unobstructed. The PMOPMI showed a great potential for asphaltene removal from solution by the combined adsorption and photocatalytic processes, being more efficient than inorganic standards, such as TiO_2 or mesoporous SiO_2 (SBA-15). The photocatalytic effect of PMOPMI can be attributed mainly to the formation of triplet state PMI, which reacts with dissolved oxygen to give reactive oxygen species that degrade the asphaltenes.

CRediT authorship contribution statement

Luana dos Santos Andrade: Investigation, Methodology, Formal analysis, Writing - review & editing. **Larissa Otubo:** Investigation, Formal analysis. **Bruna Castanheira:** Investigation, Methodology, Formal analysis. **Sergio Brochsztain:** Writing - original draft, Supervision, Project administration, Funding acquisition.

Declaration of competing interest

The authors declare that they have no known competing financial interests or personal relationships that could have appeared to influence the work reported in this paper.

Acknowledgements

S. B. acknowledges the support of FAPESP (grant No 2016/05496-2). The authors are grateful to the Multiuser Central Facilities (UFABC) for the experimental support.

Appendix A. Supplementary data

Supplementary data to this article can be found online at https://doi.org/10.1016/j.micromeso.2020.110740.

References

[1] L.-C. Hu, K.J. Shea, Organo–silica hybrid functional nanomaterials: how do organic bridging groups and silsesquioxane moieties work hand-in-hand? Chem. Soc. Rev. 40 (2011) 688–695.
[2] J.G. Croissant, X. Cattoën, J.-O. Durand, M. Wong, C. Manc, N.M. Khashab, Organosilica hybrid nanomaterials with a high organic content: syntheses and applications of silsesquioxanes, Nanoscale 8 (2016) 19945–19972.
[3] F. Hoffmann, M. Cornelius, J. Morell, M. Fröba, Silica-based mesoporous organic–inorganic hybrid materials, Angew. Chem. Int. Ed. vol. 45 (2006) 3216–3251.
[4] W. Wang, J.E. Lofgreen, G.A. Ozin, Why PMO? Towards functionality and utility of periodic mesoporous organosilicas, Small 6 (2010) 2634–2642, https://doi.org/10.1002/smll.201000617.
[5] N. Mizoshita, T. Tani, S. Inagaki, Syntheses, properties and applications of periodic mesoporous organosilicas prepared from bridged organosilane precursors, Chem. Soc. Rev. 40 (2011) 789–800.
[6] P. Van Der Voort, D. Esquivel, E. De Canck, F. Goethals, I. Van Driessche, F. J. Romero-Salguero, Periodic mesoporous organosilicas: from simple to complex bridges; a comprehensive overview of functions, morphologies and applications, Chem. Soc. Rev. 42 (2013) 3913–3955.
[7] S.S. Park, M.S. Moorthy, C.-S. Ha, Periodic mesoporous organosilicas for advanced applications, NPG Asia Mater. 6 (2014) e96, https://doi.org/10.1038/am.2014.13.
[8] F. Würthner, C.R. Saha-Möller, B. Fimmel, S. Ogi, P. Leowanawat, D. Schmidt, Perylene bisimide dye assemblies as archetype functional supramolecular materials, Chem. Rev. 116 (3) (2016) 962–1052.
[9] D. Gosztola, M.P. Niemczyk, W. Svec, A.S. Lukas, M.R. Wasielewski, Excited doublet states of electrochemically generated aromatic imide and diimide radical anions, J. Phys. Chem. A 104 (2000) 6545–6551.
[10] M.A. Kobaisi, S.V. Bhosale, K. Latham, A.M. Raynor, S.V. Bhosale, Functional naphthalene diimides: synthesis, properties, and applications, Chem. Rev. 116 (19) (2016) 11685–11796.
[11] A. Nowak-Król, K. Shoyama, M. Stolteb, F. Würthner, Naphthalene and perylene diimides – better alternatives to fullerenes for organic electronics? Chem. Commun. 54 (2018) 13763–13772.
[12] Q. Zheng, J. Huang, A. Sarjeant, H.E. Katz, Pyromellitic diimides: minimal cores for high mobility n-channel transistor semiconductors, J. Am. Chem. Soc. 130 (2008) 14410–14411.
[13] X. Zhan, A. Facchetti, S. Barlow, T.J. Marks, M.A. Ratner, M.R. Wasielewski, S. R. Marder, Rylene and related diimides for organic electronics, Adv. Mater. 23 (2011) 268–284.
[14] F.L. Castro, J.G. Santos, G.J.T. Fernandes, A.S. Araujo, V.J. Fernandes Jr., M. J. Politi, S. Brochsztain, Solid state fluorescence of a 3,4,9,10-perylenetetracarboxylic diimide derivative encapsulated in the pores of mesoporous silica MCM-41, Microporous Mesoporous Mater. 102 (2007) 258–264.
[15] F.J. Trindade, J.F.Q. Rey, S. Brochsztain, Covalent attachment of 4-amino-1,8-naphthalimides onto the walls of mesoporous molecular sieves MCM-41 and SBA-15, Dyes Pigments 89 (2011) 97–104.
[16] F.J. Trindade, J.F.Q. Rey, S. Brochsztain, Modification of molecular sieves MCM-41 and SBA-15 with covalently grafted pyromellitimide and 1,4,5,8-naphthalenediimide, J. Colloid Interface Sci. 368 (2012) 34–40.
[17] F.J. Trindade, E.R. Triboni, B. Castanheira, S. Brochsztain, Color-tunable fluorescence and white light emission from mesoporous organosilicas based on energy transfer from 1,8-naphthalimide hosts to perylenediimide guests, J. Phys. Chem. C 119 (2015) 26989–26998.
[18] M.A. Wahab, H. Hussain, C. He, Photoactive perylenediimide-bridged silsesquioxane functionalized periodic mesoporous organosilica thin films (PMO-SBA15): synthesis, self-assembly, and photoluminescent and enhanced mechanical properties, Langmuir 25 (2009) 4743–4750.
[19] N. Mizoshita, T. Tani, H. Shinokubo, S. Inagaki, Mesoporous organosilica hybrids consisting of silica-wrapped π-π stacking columns, Angew. Chem. Int. Ed. 51 (2012) 1156–1160.
[20] B. Castanheira, E.R. Triboni, L.S. Andrade, F.J. Trindade, L. Otubo, A.C.S. C. Teixeira, M.J. Politi, T.B. Queiroz, S. Brochsztain, Synthesis of novel periodic mesoporous organosilicas containing 1,4,5,8-naphthalenediimides within the pore walls and their reduction to generate wall-embedded free radicals, Langmuir 34 (2018) 8195–8204.
[21] T.B.F. Moraes, M.F.R.A. Schimidt, R. Bacani, G. Weber, M.J. Politi, B. Castanheira, S. Brochsztain, F.A. Silva, G.J.-F. Demets, E.R. Triboni, Polysilsesquioxane naphthalenediimide thermo and photochromic gels, J. Lumin. 204 (2018) 685–691.
[22] D. Zhao, Q. Huo, J. Feng, B.F. Chmelka, G.D. Stucky, Nonionic triblock and star diblock copolymer and oligomeric surfactant syntheses of highly ordered, hydrothermally stable, mesoporous silica structures, J. Am. Chem. Soc. 120 (1998) 6024–6036.
[23] S.-I. Kato, T. Matsumoto, K. Ideta, T. Shimasaki, K. Goto, T. Shinmyozu, Supramolecular assemblies and redox modulation of pyromellitic diimide-based cyclophane via noncovalent interactions with naphthol, J. Org. Chem. 71 (13) (2006) 4723–4733.
[24] J.H. Wengrovius, V.M. Powell, J.L. Webb, Synthesis of [(Trialkoxysilyl)propyl] imides, J. Org. Chem. 59 (1994) 2813–2817.
[25] S. Pfeifer, A. Schwarzer, D. Schmidt, E. Brendler, M. Veith, E. Kroke, Precursors for pyromellit-bridged silica sol–gel hybrid materials, New J. Chem. 37 (2013) 169–180.
[26] S.T. Hobson, K.J. Shea, Bridged bisimide polysilsesquioxane Xerogels: new hybrid organic-inorganic materials, Chem. Mater. 9 (1997) 616–623.
[27] T. Ribeiro, C. Baleizão, J.P.S. Farinha, Synthesis and characterization of perylenediimide labeled Core−Shell hybrid Silica−Polymer nanoparticles, J. Phys. Chem. C 113 (2009) 18082–18090.

[28] H. Rathnayake, J. Binion, A. McKee, D.J. Scardino, N.I. Hammer, Perylenediimide functionalized bridged-siloxane nanoparticles for bulk heterojunction organic photovoltaics, Nanoscale 4 (2012) 4631–4640.
[29] S. Pfeifer, E. Brendler, M. Veith, E. Kroke, Hybrid-coatings derived from pyromellitic acid bridged alkoxy-silylalkyl precursors, J. Sol. Gel Sci. Technol. 70 (2014) 191–202.
[30] C. Schramm, B. Rinderer, R. Tessadri, Ladder-like aromatic imide-functionalized poly(silsesquioxane): preparation and characterization via the sol–gel route, Adv. Polym. Technol. 36 (2015) 21576, https://doi.org/10.1002/adv.21576.
[31] C.-C. Chang, W.-C. Chen, Synthesis and optical properties of polyimide-silica hybrid thin films, Chem. Mater. 14 (10) (2002) 4242–4248.
[32] C.-C. Chang, K.-H. Wei, W.-C. Chen, Spin-coating of polyimide-silica hybrid optical thin films, J. Electrochem. Soc. 150 (2003) F147.
[33] K.A. Cychosz, R. Guillet-Nicolas, J. García-Martínez, M. Thommes, Recent advances in the textural characterization of hierarchically structured nanoporous materials, Chem. Soc. Rev. 46 (2017) 389–414.
[34] L.S. Andrade, B. Castanheira, S. Brochsztain, Periodic mesoporous organosilicas containing naphthalenediimides within the pore walls for asphaltene adsorption, Microporous Mesoporous Mater. 294 (2020) 109909.
[35] O.C. Mullins, E.Y. Sheu, A. Hammami, A.G. Marshall, Asphaltenes, Heavy Oils, and Petroleomics, Springer-Verlag, New York, 2007.
[36] J.J. Adams, Asphaltene adsorption, a literature review, Energy Fuels 28 (2014) 2831–2856, https://doi.org/10.1021/ef500282p.
[37] L.A. Calzada, R. Castellanos, L.A. García, T.E. Klimova, TiO2, SnO2 and ZnO catalysts supported on mesoporous SBA-15 versus unsupported nanopowders in photocatalytic degradation of methylene blue, Microporous Mesoporous Mater. 285 (2019) 247–258.
[38] N.N. Nassar, A. Hassan, P. Pereira-Almao, Effect of surface acidity and basicity of aluminas on asphaltene adsorption and oxidation, J. Colloid Interface Sci. 360 (2011) 233–238.
[39] A. Walcarius, L. Mercier, Mesoporous organosilica adsorbents: nanoengineered materials for removal of organic and inorganic pollutants, J. Mater. Chem. 20 (2010) 4478–4511.
[40] C.B. Vidal, A.L. Barros, C.P. Moura, A.C.A. Lima, F.S. Dias, L.C.G. Vasconcellos, P. B.A. Fechine, R.F. Nascimento, Adsorption of polycyclic aromatic hydrocarbons from aqueous solutions by modified periodic mesoporous organosilica, J. Colloid Interface Sci. 357 (2011) 466–473, https://doi.org/10.1016/j.jcis.2011.02.013.
[41] P. Yuan, X. Li, W. Wang, H. Liu, Y. Yan, H. Yang, Y. Yue, X. Bao, Tailored design of differently modified mesoporous materials to deeply understand the adsorption mechanism for polycyclic aromatic hydrocarbons, Langmuir 34 (2018) 15708–15718, https://doi.org/10.1021/acs.langmuir.8b03299.
[42] S. Theivendran, J. Zhang, C. Tang, M. Kalantari, Z. Gu, Y. Yang, Y. Yang, E. Strounina, A. Du, C. Yu, Synthesis of biphenyl bridged dendritic mesoporous organosilica with extremely high adsorption of pyrene, J. Mater. Chem. 7 (2019) 12029–12037, https://doi.org/10.1039/c9ta01281h.
[43] X. Qian, K. Fuku, Y. Kuwahara, T. Kamegawa, K. Mori, H. Yamashita, Design and functionalization of photocatalytic systems within mesoporous silica, ChemSusChem 7 (2014) 1528–1536.
[44] N. Alarcos, B. Cohen, M. Ziółek, A. Douhal, Photochemistry and photophysics in silica-based materials: ultrafast and single molecule spectroscopy observation, Chem. Rev. 117 (2017) 13639–13720.
[45] B.M. Aveline, S. Matsugo, R.W. Redmond, Photochemical mechanisms responsible for the versatile application of naphthalimides and naphthaldiimides in biological systems, J. Am. Chem. Soc. 119 (1997) 11785–11795.
[46] J. Zhao, W. Wu, J. Sun, S. Guo, Triplet photosensitizers: from molecular design to applications, Chem. Soc. Rev. 42 (2013) 5323–5351.
[47] Y. Tao, M. Wei, D. Xia, A. Xu, X. Li, Polyimides as metal-free catalysts for organic dye degradation in the presence peroxymonosulfate under visible light irradiation, RSC Adv. 5 (2015) 98231–98240.
[48] M.P. Singh, J.B. Baruah, Photophysical properties of phthalimide and pyromellitic diimide tethered imidazolium nitrophenolate salts, Chem. Select 4 (2019) 10–16.
[49] S. Pluczyk, H. Higginbotham, P. Data, Y. Takeda, S. Minakata, The impact of replacement of nitrogen with phosphorus atom in the pyromellitic diimides on their photophysical and electrochemical properties, Electrochim. Acta 295 (2019) 801–809.
[50] C. Bathula, K. Mallikarjuna, A. Kadam, N.K. Shrestha, S. Khadtare, S.D. Mane, H. Kim, Synthesis and photophysical investigations of pyromellitic diimide based small molecules, Inorg. Chem. Commun. 102 (2019) 20–24.
[51] A.J. Greenlee, C.K. Ofosu, Q. Xiao, M.M. Modan, D.E. Janzen, D.D. Cao, Pyridinium-functionalized pyromellitic diimides with stabilized radical anion states, ACS Omega 3 (2018) 240–245.